Eur. Phys. J. Plus (2023) 138:148
https://doi.org/10.1140/epjp/s13360-023-03736-5

THE EUROPEAN PHYSICAL JOURNAL PLUS

Regular Article

Modeling and simulation of the influence of quantum dots density on solar cell properties

M. Jaouane[1,a], A. Fakkahi[1], A. Ed-Dahmouny[2], K. El-Bakkari[1], A. Turker Tuzemen[3], R. Arraoui[1], A. Sali[1], F. Ungan[4]

[1] Laboratory of Solid Physics (LPS), Faculty of Science, Dhar El Mahraz, Sidi Mohamed Ben Abdellah University, B.P. 1796 Fez, Morocco
[2] Laboratory of Intelligent Systems, Georesources and Renewable Energies (SIGER), Faculty of Sciences and Technology, Sidi Mohamed Ben Abdellah University, 2202 Fez, Morocco
[3] Department of Mathematics and Science Education, Faculty of Education, Sivas Cumhuriyet University, 58140 Sivas, Turkey
[4] Department of Physics, Faculty of Science, Sivas Cumhuriyet University, 58140 Sivas, Turkey

Received: 19 November 2022 / Accepted: 22 January 2023

Abstract Based on the finite element method using the FEniCS computing platform and python programming, we solve the Schrödinger equation within the effective mass approximation. Its solution gives us the necessary energy for an electron to transit from an intermediate band to a conduction band, as well as the distribution of probability density within the system. In this work, we have investigated the efficiency of the InAs/GaAs pyramid quantum dot intermediate band solar cell (PQD-IBSC) as a function of the structure parameters and quantum dot density. The simulation results indicated the strong dependence of the efficiency of PQD-IBSC on the confinement effect, quantum dot number or quantum dot density and coupling strength. The conversion efficiency grows from 14.4587% to the optimal efficiency 17.8807%. Generally, the best efficiency is obtained for small barrier width, large quantum dot height and great quantum dot density.

1 Introduction

Semiconductor materials that have exclusive properties are preferred in the production of photovoltaic technologies with high efficiency like solar cells. One of the nanocrystal candidate structures based on semiconductor materials used to ensure an increase in solar cell efficiency [1] is quantum dots (QDs) [2–4] because of their extraordinary electrical and optical properties. QDs are a special form of semiconductors qualified with continuous valence and conduction bands. The quantum confinement effect owned by QDs determines their electronic and optical properties. This property ensures fine-tuning on the optical properties such as absorption wavelength [5, 6] and bandgap [7]. QDs have important characteristics like narrow emission spectra, size-tunable bandgap, and long-term stability. The dependence of the bandgap on the nanocrystalline size allows researchers to tune the bandgap energy by adjusting its size. QDs have adjustable properties according to their shapes, sizes, and materials. The light is firstly absorbed and then emitted by QD when excited. The factor that determines the light's color is the dot's size. The smaller dots emit light with higher energy compared to larger dots. Another important reason why they are preferred in solar cell production is the potential of QDs to minimize losses from thermalization and unabsorbed photons. Among the QDs (cuboid, cylindrical, pyramidal, conical, and lens-shaped), pyramidal-shaped structures have different importance due to growing application areas in semiconductor device technologies (lasers, photonic structures, light detectors, and solar cells) [7–9].

QDs act as the intermediate band (IB) in solar cell structure and increase the cell's efficiency. This increase takes place because of QDs' properties about the absorbing subband gap photons by the two-photon transition between the valence band and the conduction band [10–13]. In the case of two-photon transition, the key parameter is the coupling of each QD wave function with the neighboring one to widen the discrete quantum levels for creating miniband (i.e., IB) which has finite width in the well-ordered and close-packed QDs superlattice. These intermediate band solar cell (IBSC) structure has been suggested for overcoming the loss mechanisms specified in Shockley–Queisser model [10, 14–18]. The IBSC's different from the conventional solar cell is that it increases both voltage and current using only one junction [10].

While the conventional silicon-based solar cells reach the efficiency of just over 26% [19] (nearly their fundamental limiting efficiency of 32%), IBSCs provide the theoretical power efficiency of 63% under full light concentration [15]. Theoretical solutions to these structures have mathematical difficulties, and the numerical techniques must be used to overcome these difficulties [20–22]. Considering the studies on the subject, Cuadra et.al. [23] investigated the effect of the overlap of the absorption coefficients on the intermediate band solar cell's efficiency and determined that in the case of overlap occurs the efficiency reduces. A new low-

[a] e-mail: mohammed.jaouane@gmail.com (corresponding author)

Published online: 12 February 2023

temperature characterization technique based on concentrated light is introduced by Linares et al. [16] in the case of the open-circuit voltage has been fully recovered. Lee et al. [24] have suggested an effective method to compute the structure of miniband and density of states for a well-ordered Ge/Si-nanodisk array. Their suggestion has been a guideline for three-dimensional QDs design. Another work by Lee et al. [25] studied the physical and the electrical characteristics of Ge/Si QDs based IBSC and used a new 3D finite element method to compute the miniband structure and density of state. H. El Ghazi [26] investigated the photovoltaic conversion efficiency of a one-intermediate band solar cell based on GaN/InN/GaN quantum well and showed that under full light concentration the optimum power conversion has been obtained for thin QW.

In this paper, we investigated the influence of quantum dot density, QD size and dot spacing on the parameters of PQD-IBSC based on Schrödinger equation and Luque model**.** The organization of the paper is that Sect. 2 gives the theoretical background of the numerical calculations. Section 3 discusses in detail the simulation result and compares the obtained results. Finally, a conclusion of the physical results obtained in the paper is given in Sect. 4.

2 Computational model

In this paper, we consider a model of semiconductor multi-pyramid shape, consisting of InAs QDs grown on a GaAs substrate and embedded in a three-dimensional matrix of the same material. The electron properties are described numerically in three dimensional (3D) by solving the Schrödinger equation with the effective mass approximation, that can be expressed as:

$$H\psi = \left(-\frac{\hbar^2}{2}\vec{\nabla}\left(\frac{1}{m_j^*}\vec{\nabla}\right) + V(x, y, z)\right)\psi \tag{1}$$

where $\hbar$ is the reduced Planck constant, ψ is the wavefunction, $\mathrm{m}^*{}_j$ represents the electron effective mass, having two different values in two regions, QD domain and its surrounded medium. The pyramid electron confinement potential ($V(x, y, z)$) is written as:

$$V(x, y, z) = \begin{cases} 0 & \text{if}(x, y, z) \in \text{PQD} \\ V_0 & \text{otherwise} \end{cases} \tag{2}$$

with $\mathrm{V}_0 = Q\Delta E_g$ is the conduction band discontinuity, $Q(= 0.7)$ is the conduction band offset and $\Delta E_g = E_{\mathrm{GaAs}} - E_{\mathrm{InAs}}$ is the gap energy difference between GaAs matrix and InAs QD material. The presence of QD creates a miniband between the conduction band (CB) and the valence band (VB), the miniband is called the intermediate band solar cell (IBSC). To study the properties of IBSC based on InAs/GaAs material, with different PQDs numbers, we adopted the Luque model [10, 27] with consideration of QD density to calculate the current density and conversion efficiency (CE), the current density which characterizes the PQD-IBSC is expressed as [28]:

$$J = J_{\mathrm{CV}}(\mu_{\mathrm{CV}}) + \tau \times J_{\mathrm{IB}}(\mu_{\mathrm{CI}}, \mu_{\mathrm{IV}}) \tag{3}$$

where τ is the ratio of the PQD volume and the bulk material that creates an additional current density from intermediate band (IB), the photocurrent density J_{IB} is written as:

$$J_{\mathrm{IB}} = e(G_{\mathrm{CI}} - R_{\mathrm{CI}}(\mu_{\mathrm{CI}})). \tag{4}$$

The photocurrent density induced by the bulk material is given as [28]:

$$J_{\mathrm{CV}} = e(G_{\mathrm{CV}} - R_{\mathrm{CV}}(\mu_{\mathrm{CV}})) \tag{5}$$

Here, G_{CV} and G_{CI} are the electron generation rates related to transitions VB $\rightarrow$ CB and IB $\rightarrow$ CB, respectively, and are given by [28, 29]:

$$G = \frac{\chi\Omega_s}{\pi}\int f(E, T_{\mathrm{s}}, 0)\mathrm{d}E + \left(1 - \frac{\chi\Omega_s}{\pi}\right)\int f(E, T_c, 0)\mathrm{d}E, \tag{6}$$

where $\chi(1000)$ is a concentration factor, $T_{\mathrm{s}}(5778K)$ is the temperature of sun, $T_{\mathrm{c}}(300K)$ is the temperature of solar cell [28], $\Omega_S = \pi\sin(\theta)^2$ is a geometrical factor, θ corresponds to the angle between the sun rays and a vector normal to the panel surface, for the sun as seen from the earth, in this case $\theta \approx 0.26^{\circ}$ [27, 30]. The flux photon density emitted or absorbed is expressed by [26]:

$$\int f(E, T, \mu)\mathrm{d}E = \frac{2\pi}{h^3c^2}\int \frac{E^2}{e^{(E-\mu)/k_{\mathrm{b}}T} - 1}\mathrm{d}E \tag{7}$$

where h is the Planck constant, c is the light velocity and k_{b} is the Boltzmann constant. The electrons recombination rites due to transitions VB $\rightarrow$ CB and IB $\rightarrow$ CB are noted as R_{CV} and R_{CI}, respectively.

$$R(\mu_{\mathrm{if}}) = \int f(E, T, \mu_{\mathrm{if}})\mathrm{d}E \tag{8}$$

with μ_{if} is the quasi-fermi energy difference between two minibands i and f. For a given output voltage V, the quasi-fermi energies μ_{CV}, μ_{CI} and μ_{IV} are related by the following equation:

$$qV = \mu_{\text{CV}} = \mu_{\text{CI}} + \mu_{\text{IV}} \tag{9}$$

with q is the electron charge. As no current is induced from the one intermediate band, the current density entering and leaving this band must be equal [10, 29]:

$$G_{\text{CI}} - R_{\text{CI}}(\mu_{\text{CI}}) = G_{\text{IV}} - R_{\text{CI}}(\mu_{\text{IV}}) \tag{10}$$

So, the equation takes the form,

$$\begin{aligned} & e\left[\frac{\chi\Omega_s}{\pi}\int_{E_{\text{c}}}^{E_{\text{g}}} f(E,T_{\text{s}},0)\text{d}E + \left(1-\frac{\chi\Omega_{\text{s}}}{\pi}\right)\int_{E_{\text{c}}}^{E_{\text{g}}} f(E,T_c,0)\text{d}E - \int_{E_{\text{c}}}^{E_{\text{g}}} f(E,T_{\text{c}},\mu_{CI})\text{d}E\right] \\ & = e\left[\frac{\chi\Omega_S}{\pi}\int_{E_{\text{I}}}^{E_{\text{c}}} f(E,T_{\text{s}},0)\text{d}E + \left(1-\frac{\chi\Omega_S}{\pi}\right)\int_{E_{\text{I}}}^{E_{\text{c}}} f(E,T_{\text{s}},0)\text{d}E - \int_{E_{\text{I}}}^{E_{\text{c}}} f(E,T_{\text{c}},\mu_{\text{IV}})\text{d}E\right] \end{aligned} \tag{11}$$

where $E_{\text{c}} = E_{\text{g}} - E_{\text{I}}$, E_g is the band gap and E_{I} is the intermediate band energy level. The two unknown quasi-fermi energies μ_{CI} and μ_{IV} can be obtained from the solution of the two equations (9, 11) for a given output voltage V.

The conversion efficiency of one intermediate band photovoltaic solar cell η is expressed by using the following parameters**:** the open-circuit voltage V_{oc}, the short circuit current (I_{scc}), and V_{m} and I_{m} that correspond to the operating point of the $I-V$ characteristic that maximizes the output power. It is formulated as [26]:

$$\eta = \frac{\text{V}_{\text{oc}}\text{J}_{\text{scc}}FF}{P_{\text{in}}} \tag{12}$$

where, $P_{in} = \sigma_s T_s^4$ is the incoming power density at sun surface, with $\sigma_{\text{s}} = 5.67 \times 10^{-8} Wm^{-2}K^{-4}$ is the Stefan–Boltzmann constant. The essential parameter for measuring the performance of solar cells is known as the fill factory (FF), is given by:

$$\text{FF} = \frac{V_{\text{m}}I_{\text{m}}}{V_{\text{oc}}I_{\text{scc}}}. \tag{13}$$

3 Results and discussions

With FEniCS project, Python programming language and the effective mass approximation, we succeeded to solve the Schrödinger equation that describes the electron properties in the 3D complicated geometry. The necessary physical parameters in this work are $m^*_{\text{InAs}} = 0.023m_{\text{e}}$, $m^*_{\text{GaAs}} = 0.067\text{m}_{\text{e}}$, $E_{\text{g, InAs}} = 0.354$ eV, $E_{\text{g, GaAs}} = 1.424$ eV and $\varepsilon_{\text{InAs}} = 15.15$ [31–33]. The Fig. 1 portrayed the schematic view of the one, five and nine PQDs structures with a using mesh (see Table 1) for solving the Schrödinger equation. The average execution time for one electron energy ground state is about 7 h by using a computer with an 8 Go RAM and a Processor Intel(*R*) Core (TM) i7-6600U CPU @ 2.60 GHz, 2808 MHz, 2 Core(s), 4 Logical Processor(s).

The intermediate band solar cell is determined by the energy of an electron confined inside a QD material sandwiched in material barrier. From this result, we can have knowledge of the necessary energy of an electron for transit from the intermediate band to the conduction band.

The confinement factors that can affect strongly the intermediate band are the barrier width s and pyramid height h_{d}. To evaluate the impact of confinement on the intermediate band, we have investigated in Fig. 2 the relationship between electron energy ground state (EEGS) in InAs/GaAs PQD and coupling strength, which is tunable by two factors the barrier width s and QD numbers. Where QD number is taken one, five and nine QDs**,** the corresponding to the quantum dot density (QDD) are $D_1 = 1.8903 \times 10^{11}\text{cm}^{-2}$, $D_5 = 5 \times D_1$ and $D_9 = 9 \times D_1$ at $s = 2$ nm, respectively. This result is measured for the case of $l_{\text{p}} = 5$ nm, $h_{\text{p}} = 5$ nm, $s = 2$ nm, $w_{\text{l}} = 0.6$ nm and $h_{\text{b}} = 10$ nm. As can be seen from this figure, for a fixed barrier width, there is a regular increase in EEGS as QDD decreases. On the other side, when we have only one QD, the EEGS approximately remains the same value for all barrier widths because of the absence of coupling effect. However, for five and nine QDs, the EEGS changes to a high value as the barrier width s is expanded until it converges to the energy of one QD. The physics argument is as follows, for an independent QD, the probability density is localized inside the QD, so the electron is more confined in this case, as a consequence the energy takes an important value. For five and nine QDs, the results of EEGS can be explained by the coupling effect between QDs, as the dot spacing is small,

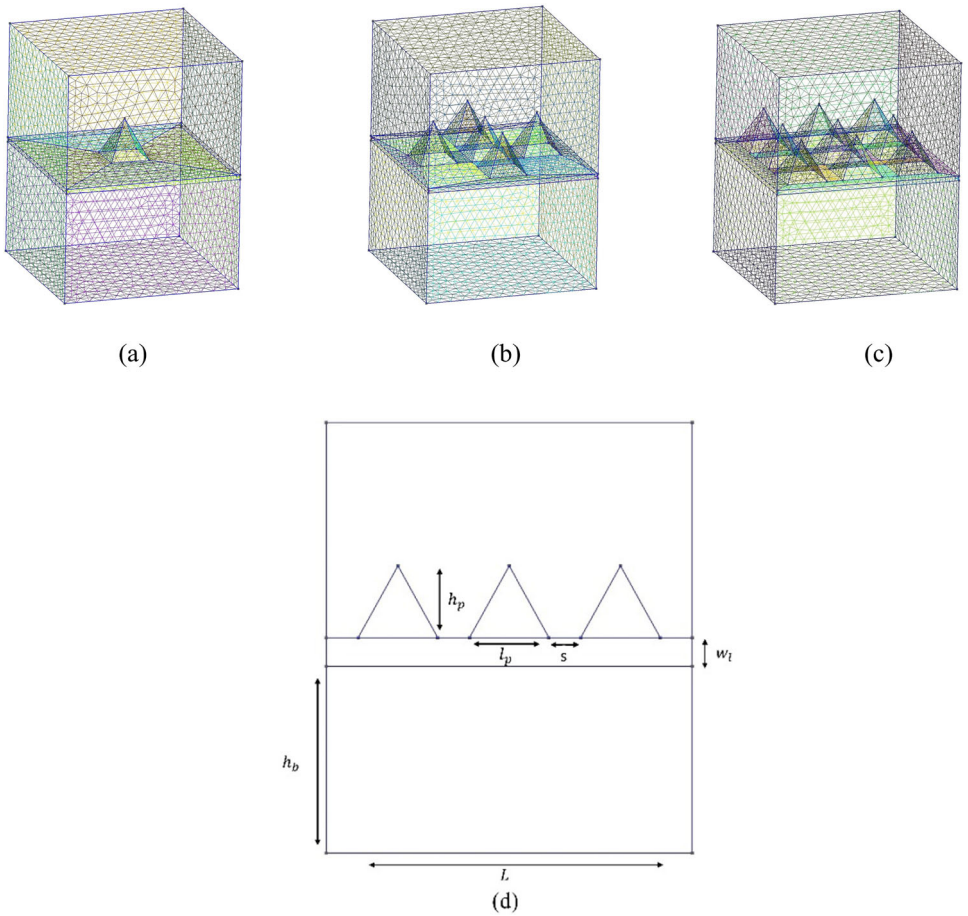

Fig. 1 Schematic illustration for 3D square pyramid base quantum dots, **a** one quantum dot, **b** five quantum dots, **c** nine quantum dots and **d** the x-axis view of nine QDs system with $l_{\mathrm{p}} = 5$ nm, $h_{\mathrm{p}} = 5$ nm, $s = 2$ nm, $w_{\mathrm{l}} = 0.6$ nm and $h_{\mathrm{b}} = 10$ nm

Table 1 The mesh element for MPQDs with $l_{\mathrm{p}} = 5$ nm, $h_{\mathrm{p}} = 5$ nm, $s = 2$ nm, $w_l = 0.6$ nm and $h_{\mathrm{b}} = 10$ nm

	Nodes	Lines	Triangles	Tetrahedra
One QD	6086	489	6542	29,872
Five QDs	8686	829	8642	45,513
Nine QDs	8221	1029	9022	42,621

the coupling effect among the QDs is strong and the wavefunction is penetrated into regions between QDs, so the electron can move among the QDs. So, the diminishing of quantum confinement causes a reducing in EEGS. Otherwise, as the barrier width increases, the coupling effect reduces and electron movement becomes more restricted. Furthermore, for large barrier width the coupling effect is weak and the QDs in the system acts like an independent QD, so the electron is mainly located inside each QD, as a result the energy for three cases approaches to each other. To verify the outcomes of our numerical investigation on PQD, we illustrated in Fig. 3 the ground state probability (GSP) of an electron for three cases, one, five and nine QDs for two barrier width $s = 1$ nm and $s = 3$ nm, these results match well with the earlier work [34–36].

With the previous parameters and fixed barrier width at 2 nm, we reveal in Fig. 4 the effect of pyramid height h_p on the EEGS for one, five and nine QDs. The calculated EEGS is proportional to the maximum transition energy from the intermediate band to the conduction band, the energy decreases gradually with increasing h_{d}, so the QD size has a great effect on EEGS. The reduction in the energy is related to the confinement effect that vanishes progressively with an increment of the pyramid height. These results are in agreement with the reference [34].

Now, let us discuss the impact of QD density, coupling strength and confinement effect on parameters that determine the PQD-IBSC performance: V_{oc}, I_{scc}, V_{m} and I_{m}, for this purpose, we simulated $J - V$ profile of InAs/GaAs PQD-IBSC under 1000 sun

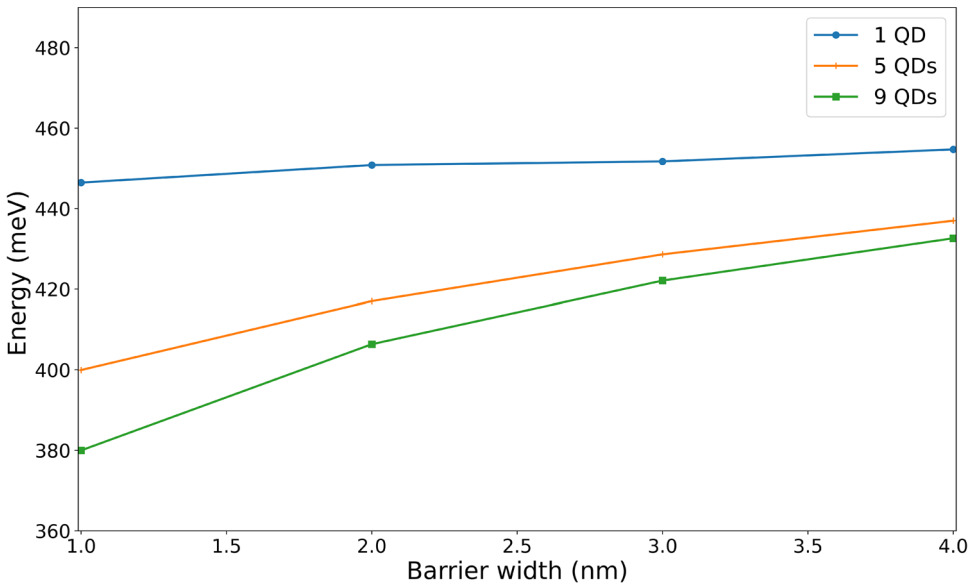

Fig. 2 Electron energy as a function of barrier width (s) for three cases: one, five and nine QDs with $l_{\mathrm{p}} = 5$ nm, $w_{\mathrm{l}} = 0.6$ nm and $h_b = 10$ nm

illumination. Figure 5 displays the current densities induced from the intermediate band and the system as a function of external voltage V for various QD numbers, one, five and nine. As seen in this figure, the current density is sensitive to the QD density, the presence of QD increases the current density more specifically the short circuit current in comparing with bulk material, meanwhile the open-circuit voltage value is unaffected. These outcomes can be explained by the following physical reasons, in the bulk material, we have only one transition from the VB to the CB with an energy greater than $E_{g,GaAs}$. The presence of QDs creates an intermediate band between VB and CB, which makes an additional transition possible with an energy less than $E_{\mathrm{g,GaAs}}$ as a consequence the current density rises. To be more realistic, from this figure, we calculate the conversion efficiency as shown in Table 2. In the absence of QD, the efficacity conversation is taken a constant value about 14.4587%, meanwhile, the presence of one, five or nine QD change gradually the CE to $\eta(1QD) = 15.1133\%$, $\eta(5QDs) = 15.9834\%$ and $\eta(9QDs) = 16.9242\%$.

In Fig. 6, we reported the current density associated with the system as a function of the external voltage V. In this case, we plot J in units of $\mathrm{mA} \cdot \mathrm{cm}^{-2}$ for three different barrier widths $s = 1$ nm, 2 nm and 4 nm. It is interesting to note that with a decrease in the barrier width, the current density J starts to take an important value and the open circuit voltage keeps the same value, so the current density can be manipulated much strongly by the coupling effect that is related to barrier width, as shown in Fig. 3. In order to analyze the effect of barrier width, we have presented in Table 3 the conversion efficiency as a function of barrier width s. As we can see, the conversion efficiency is increment as the barrier width is diminished. This result can be explained by the following reasons, when the QD is closed together, the electron wave function penetrates into the barrier region, so the electron can move among the QDs as shown by the probability density that is presented in Fig. 2 and the discussion part of Fig. 3. Furthermore, for reduced barrier width, the coefficient absorption takes important values, as mentioned in the work [37], it contributed in the growth of the current density and the conversion efficiency. The results of our study are consistent with the findings of previous research [38].

This graph (Fig. 7) illustrates the change of the current density J for nine QDs versus the external voltage V, for different values of pyramid height values $h_{\mathrm{p}} = 3$ nm, 5 nm, 7 nm and 9 nm. It is obvious that the current density J is increment as the pyramid height is expanded, this result can be interpreted by the important contribution of h_{p} on ρ that presents the ratio of the PQD to volume of bulk material. In addition, as the volume of QDs rises, more photons are absorbed, as a consequence, exciting more electrons. In order to discuss the efficiency of solar cells, we exported from Fig. 7 in the Table 4, the conversion efficiency, one can notice that a regular increment of h_{p}: $h_{\mathrm{p}} = 3$ nm, 5 nm, 7 nm and 9 nm makes the CE takes16.4207%, 16.9242%, 17.3236%, and 17.6321%, respectively.

4 Conclusion

By using the finite element method and the Python programming language, we were able to solve the Schrödinger equation in 3D complicated geometry, which consists of InAs square pyramid quantum dots and GaAs barrier material. The presence of quantum dots creates a miniband that works as an intermediate band, this miniband is determined by the solution of the equation. In this current investigation, we explore the impact of quantum dot density, quantum dot size and strength coupling (dot spacing) on the parameters that adjust the conversion efficiency of pyramid quantum dot intermediate band solar cell. The presence of quantum dot changes considerably the performance of intermediate band solar cell, which alters the conversion efficiency to high values as the

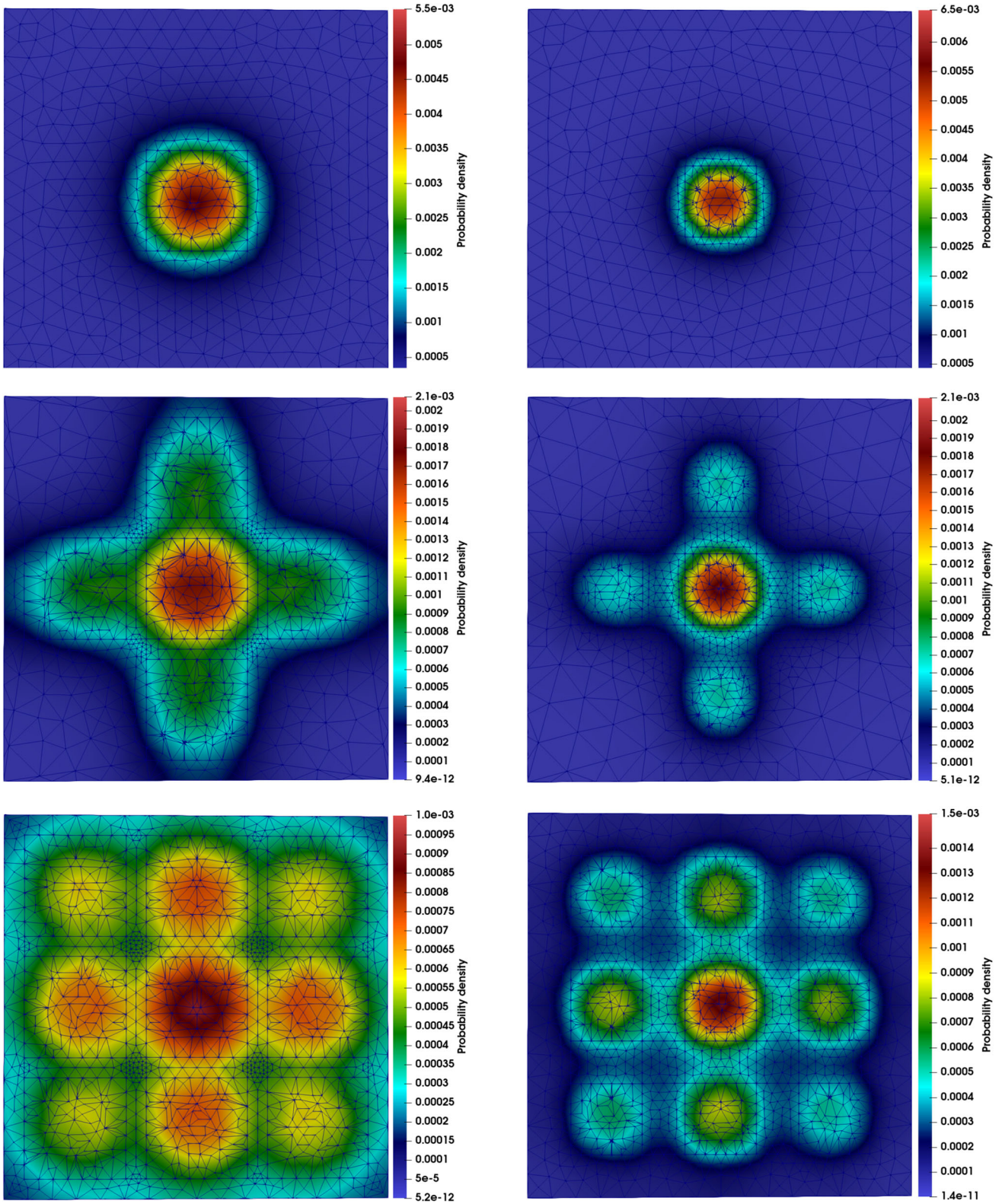

Fig. 3 Ground state probability density of an electron in multi-pyramid quantum dots, for three cases one (above), five (middle) and nine (below) QDs with two different barrier widths $s = 1$ nm (left) and 3 nm (right) with $l_{\mathrm{p}} = 5$ nm, $h_{\mathrm{p}} = 5$ nm, $w_{\mathrm{l}} = 0.6$ nm and $h_{\mathrm{b}} = 10$ nm

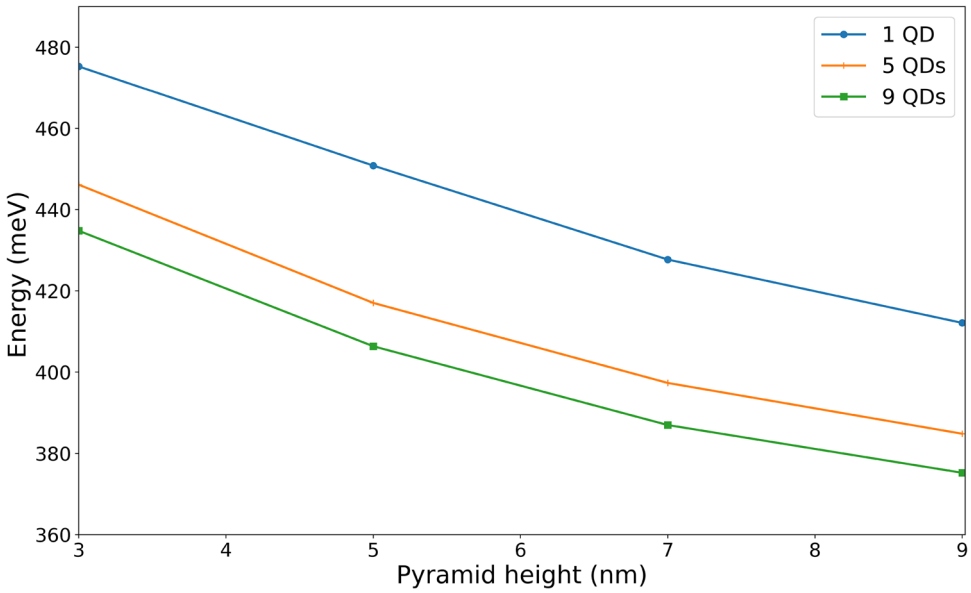

Fig. 4 Electron energy as a function of pyramid height (h_p) for three cases: one, five and nine QDs with $l_p = 5$ nm, $s = 2$ nm, $w_l = 0.6$ nm and $h_b = 10$ nm

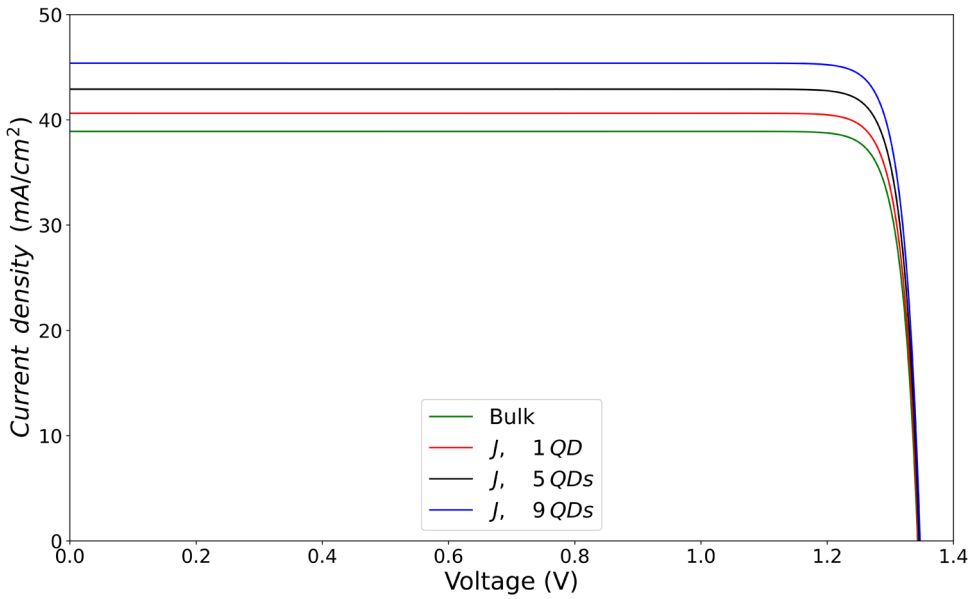

Fig. 5 Current density induced from the system J as a function of external voltage V with different cases: one, five and nine QDs with $l_p = 5$ nm, $h_p = 5$ nm, $s = 2$ nm, $w_l = 0.6$ nm and $h_b = 10$ nm

Table 2 Photovoltaic conversion efficiencies η_M(bulk), η (system), fill factor FF_M(bulk) and FF (system) as a function of quantum dot numbers with $l_p = 5$ nm, $h_p = 5$ nm, $s = 2$ nm, $w_l = 0.6$ nm and $h_b = 10$ nm

	$\eta_M(\%)$	FF_M	$\eta(\%)$	FF
1QD	14.4587	0.9066	15.1133	0.9067
5QDs	14.4587	0.9066	15.9834	0.9068
9QDs	14.4587	0.9066	16.9242	0.9069

quantum dot density takes an important value. Furthermore, the quantum dot structures mainly the dot spacing s and the pyramid quantum dots height h_d affect the strength coupling among the quantum dots and quantum confinement, respectively. In this respect, the conversation efficiency of pyramid quantum dot intermediate band solar cell is tunable by these factors, as the reduction in the dot spacing or expanded of the pyramid quantum dot height, the efficiency shows an important enhancement. The highest efficiency of 17.8807% is attained for nine quantum dot, barrier width of 1 nm and pyramid quantum dot height of 5 nm.

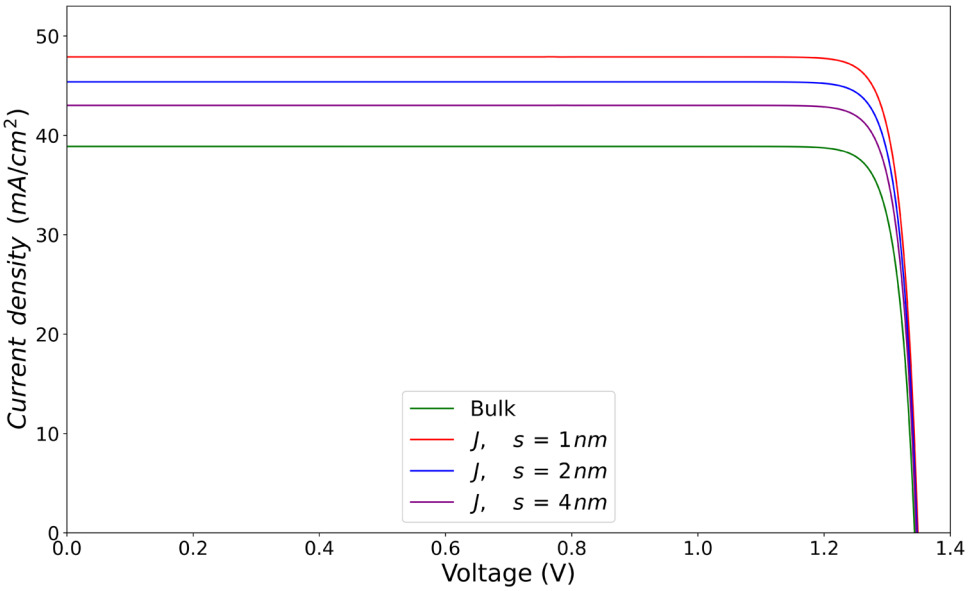

Fig. 6 Current density induced from the system J as a function of external voltage V with different barrier width values: $s = 1$ nm, 2 nm and 4 nm for nine QDs for fixed parameters, $l_{\mathrm{p}} = 5$ nm, $h_{\mathrm{p}} = 5$ nm, $w_{\mathrm{l}} = 0.6$ nm and $h_{\mathrm{b}} = 10$ nm

Table 3 Photovoltaic conversion efficiencies η_M(bulk), η (system) and fill factor FF (system) as a function of barrier width s QDs with $l_{\mathrm{p}} = 5$ nm, $h_{\mathrm{p}} = 5$ nm, $w_{\mathrm{l}} = 0.6$ nm and $h_{\mathrm{b}} = 10$ nm

	$\eta_M(\%)$	$\eta(\%)$	FF
$s = 1$ nm	14.4587	17.8807	0.90700
$s = 2$ nm	14.4587	16.9242	0.90690
$s = 4$ nm	14.4587	16.0251	0.90681

Table 4 Photovoltaic conversion efficiencies η_M(bulk), η (system) and fill factor FF (system) as a function of pyramid height h_{p} with $l_{\mathrm{p}} = 5$ nm, $s = 2$ nm, $w_{\mathrm{l}} = 0.6$ nm and $h_{\mathrm{b}} = 10$ nm

	$\eta_M(\%)$	$\eta(\%)$	FF
$h_{\mathrm{p}} = 3$nm	14.4587	16.4207	0.90685
$h_{\mathrm{p}} = 5$nm	14.4587	16.9242	0.90690
$h_{\mathrm{p}} = 7$nm	14.4587	17.3236	0.90695
$h_{\mathrm{p}} = 9$nm	14.4587	17.6321	0.90698

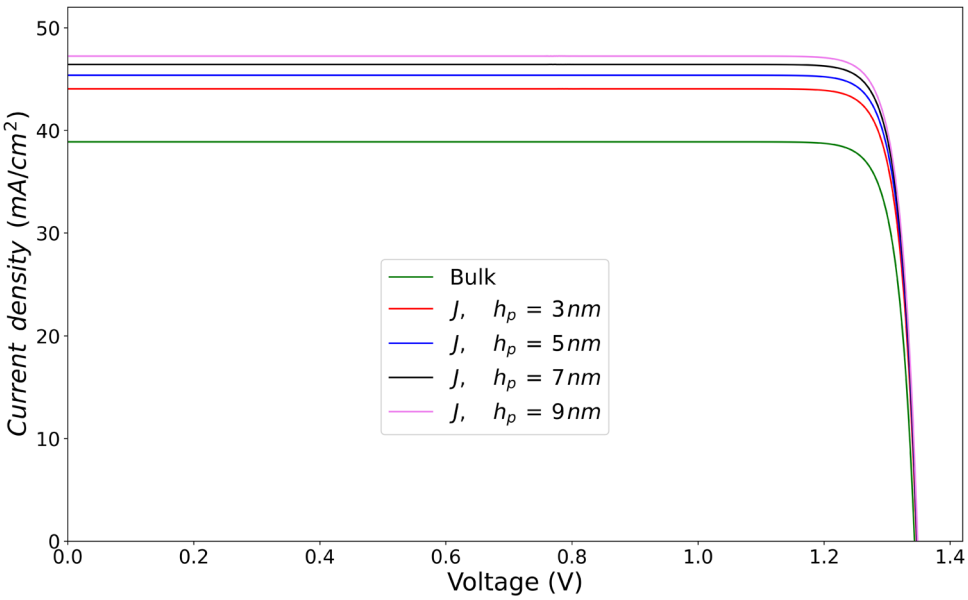

Fig. 7 Current density induced from the system as a function of external voltage V with different pyramid heights $h_{\mathrm{p}} = 3$ nm, 5 nm, 7 nm and 9 nm for nine QDs, $l_{\mathrm{p}} = 5$ nm, $s = 2$ nm, $w_{\mathrm{l}} = 0.6$ nm and $h_{\mathrm{b}} = 10$ nm

Acknowledgements This work was supported by the National Centre for Scientific and Technical Research (NCSTR) in Morocco.

Author contribution M. Jaouane, F. Ungan and A. Sali contributed to conceptualization, acquisition of data, formal analysis, drafting the manuscript, revising the manuscript critically for important intellectual content, approval of the version of the manuscript to be published; M. Jaouane, A. Fakkahi, A. Ed-Dahmouny, and A. Sali contributed to conceptualization, acquisition of data, formal analysis, drafting the manuscript, revising the manuscript critically for important intellectual content, approval of the version of the manuscript to be published; M. Jaouane, A. Turker Tuzemen, R. Arraoui and F. Ungan contributed to conceptualization, formal analysis, approval of the version of the manuscript to be published.

Data Availability Statement This manuscript has associated data in a data repository. [Authors' comment: All data included in this manuscript are available upon request by contacting with the corresponding author.]

Declarations

Conflict of interest The authors declare that they have no known competing financial interests or personal relationships that could have appeared to influence the work reported in this paper.

References

1. M.A. Danandeh, S.M. Mousavi G, Comparative and comprehensive review of maximum power point tracking methods for PV cells. Renew. Sustain. Energy Rev. **82**, 2743–2767 (2018). https://doi.org/10.1016/j.rser.2017.10.009
2. M.A. Green, *Third Generation Photovoltaics* (Springer, Berlin, 2006)
3. W. Hu, M. Igarashi, M. Lee, Y. Li, S. Samukawa, 50% Efficiency intermediate band solar cell design using highly periodical silicon nanodisk array, in *2012 International Electron Devices Meeting (*IEEE, 2012). https://doi.org/10.1109/IEDM.2012.6478987.
4. H. Abboudi, H. El Ghazi, F. Benhaddou, R. En-Nadir, A. Jorio, I. Zorkani, Temperature-related photovoltaic characteristics of (In, Ga)N single-intermediate band quantum well solar cells for different shapes. Phys. B Condens. Matter. (2022). https://doi.org/10.1016/j.physb.2021.413495
5. P. Guyot-Sionnest, Colloidal quantum dots. Comptes Rendus Phys. **9**, 777–787 (2008). https://doi.org/10.1016/j.crhy.2008.10.006
6. H. Zhao, F. Rosei, Colloidal quantum dots for solar technologies. Chem **3**, 229–258 (2017). https://doi.org/10.1016/j.chempr.2017.07.007
7. X. Xin, *Quantum Dot Solar Cells*, 1st edn. (Springer, New York, 2014)
8. G.C. Tiriba, E.C. Niculescu, L.M. Burileanu, Hydrostatic pressure and magnetic field effects on donor states in pyramidal quantum dots. Superlattices Microstruct. **75**, 749–760 (2014). https://doi.org/10.1016/j.spmi.2014.09.010
9. A. Baranov, E. Tournié, *Semiconductor Lasers*, 1st edn. (Woodhead Publishing Limited, Cambridge, 2013)
10. A. Luque, A. Martí, Increasing the efficiency of ideal solar cells by photon induced transitions at intermediate levels. Phys. Rev. Lett. **78**, 5014–5017 (1997). https://doi.org/10.1103/PhysRevLett.78.5014
11. A. Luque, A. Martí, C. Stanley, Understanding intermediate-band solar cells. Nat. Photon **6**, 146–152 (2012). https://doi.org/10.1038/nphoton.2012.1
12. A.S. Lin, W. Wang, J.D. Phillips, Model for intermediate band solar cells incorporating carrier transport and recombination. J. Appl. Phys. **105**, 064512 (2009). https://doi.org/10.1063/1.3093962
13. A.M. Kechiantz, L.M. Kocharyan, H.M. Kechiyants, Band alignment and conversion efficiency in Si/Ge type-II quantum dot intermediate band solar cells. Nanotechnology. **18**, 405401 (2007). https://doi.org/10.1088/0957-4484/18/40/405401
14. W. Shockley, H.J. Queisser, Detailed balance limit of efficiency of p-n junction solar cells. J. Appl. Phys. **32**, 510–519 (1961). https://doi.org/10.1063/1.1736034
15. P.G. Linares, C.D. Farmer, E. Antolín, S. Chakrabarti, A.M. Sánchez, T. Ben, S.I. Molina, C.R. Stanley, A. Martí, A. Luque, Inx(GayAl1-y)1-xAs quaternary alloys for quantum dot intermediate band solar cells. Energy Procedia **2**, 133–141 (2010). https://doi.org/10.1016/j.egypro.2010.07.019
16. P.G. Linares, A. Martí, E. Antolín, C.D. Farmer, Í. Ramiro, C.R. Stanley, A. Luque, Voltage recovery in intermediate band solar cells. Sol. Energy Mater. Sol. Cells. **98**, 240–244 (2012). https://doi.org/10.1016/j.solmat.2011.11.015
17. T.A. Ameen, Y.M. El-Batawy, A.A. Abouelsaood, A theoretical study of light absorption in self assembled quantum dots. Opt. Photon. J. **03**, 243–247 (2013). https://doi.org/10.4236/opj.2013.32B057
18. Y. Okada, N.J. Ekins-Daukes, T. Kita, R. Tamaki, M. Yoshida, A. Pusch, O. Hess, C.C. Phillips, D.J. Farrell, K. Yoshida, N. Ahsan, Y. Shoji, T. Sogabe, J.-F. Guillemoles, Intermediate band solar cells: Recent progress and future directions. Appl. Phys. Rev. **2**, 021302 (2015). https://doi.org/10.1063/1.4916561
19. M. Nolan, M. Legesse, G. Fagas, Surface orientation effects in crystalline–amorphous silicon interfaces. Phys. Chem. Chem. Phys. **14**, 15173 (2012). https://doi.org/10.1039/c2cp42679j
20. T. Hwang, W. Lin, W. Wang, W. Wang, Numerical simulation of three dimensional pyramid quantum dot **196**, 208–232 (2004). https://doi.org/10.1016/j.jcp.2003.10.026
21. M. Sabaeian, M. Shahzadeh, Self-assembled strained pyramid-shaped InAs/GaAs quantum dots: the effects of wetting layer thickness on discrete and quasi-continuum levels. Phys. E Low Dimens. Syst. Nanostructss **61**, 62–68 (2014). https://doi.org/10.1016/j.physe.2014.03.015
22. R. Khordad, H. Bahramiyan, Impurity position effect on optical properties of various quantum dots. Phys. E Low Dimens. Syst. Nanostruct. **66**, 107–115 (2015). https://doi.org/10.1016/j.physe.2014.09.021
23. L. Cuadra, A. Marti, A. Luque, Influence of the overlap between the absorption coefficients on the efficiency of the intermediate band solar cell. IEEE Trans. Electron Devices. **51**, 1002–1007 (2004). https://doi.org/10.1109/TED.2004.828161
24. M.-Y. Lee, Y.-C. Tsai, Y. Li, S. Samukawa (2015) Electronic structure dependence on the density, size and shape of Ge/Si quantum dots array. in 2015 International Workshop on Computational Electronics (IEEE) https://doi.org/10.1109/IWCE.2015.7301970
25. M.Y. Lee, Y.C. Tsai, Y. Li, S. Samukawa, Numerical simulation of physical and electrical characteristics of Ge/Si quantum dots based intermediate band solar cell, in 16th IEEE 16th International Conference on Nanotechnology—IEEE NANO 2016. (2016) pp 361–364. https://doi.org/10.1109/NANO.2016.7751551
26. H. El Ghazi, Numerical investigation of one-intermediate band InN/GaN QW solar cell under electric field, impurity and size effects. Phys. B Condens. Matter. **602**, 412427 (2021). https://doi.org/10.1016/j.physb.2020.412427
27. L. Cuadra, A. Martí, A. Luque, Influence of the overlap between the absorption coefficients on the efficiency of the intermediate band solar cell. IEEE Trans. Electron Devices **51**, 1002–1007 (2004). https://doi.org/10.1109/TED.2004.828161

28. M.-Y. Lee, Y. Li, S. Samukawa, Miniband calculation of 3-D nanostructure array for solar cell applications. IEEE Trans. Electron Devices. **62**, 3709–3714 (2015). https://doi.org/10.1109/TED.2015.2474161
29. S.E. Jenks, Quantum dot intermediate band solar cells: design criteria and optimal materials (2012)
30. J. Nelson, The Physics of Solar Cells, Published by Imperial College Press and Distributed by World Scientific Publishing CO., (2003) https://doi.org/10.1142/p276
31. S.L. Chuang, *Physics of Optoelectronic Devices* (Wiley, Newyork, 1995)
32. L.R.C. Fonseca, J.L. Jimenez, J.P. Leburton, R.M. Martin, Self-consistent calculation of the electronic structure and electron-electron interaction in self-assembled InAs-GaAs quantum dot structures. Phys. Rev. B. **57**, 4017–4026 (1998). https://doi.org/10.1103/PhysRevB.57.4017
33. C. Pryor, Geometry and material parameter dependence of InAs/GaAs quantum dot electronic structure. Phys. Rev. B Condens. Matter Mater. Phys. **60**, 2869–2874 (1999). https://doi.org/10.1103/PhysRevB.60.2869
34. M. Jaouane, A. Sali, A. Ezzarfi, A. Fakkahi, R. Arraoui, Study of hydrostatic pressure, electric and magnetic fields effects on the donor binding energy in multilayer cylindrical quantum dots. Phys. E Low Dimens. Syst. Nanostruct **127**, 114543 (2021). https://doi.org/10.1016/j.physe.2020.114543
35. K. Sakamoto, Y. Kondo, K. Uchida, K. Yamaguchi, Quantum-dot density dependence of power conversion efficiency of intermediate-band solar cells. J. Appl. Phys. (2012). https://doi.org/10.1063/1.4771925
36. A. Fakkahi, A. Sali, M. Jaouane, R. Arraoui, Hydrostatic pressure, temperature, and electric field effects on the hydrogenic impurity binding energy in a multilayered spherical quantum dot. Appl. Phys. A. **127**, 908 (2021). https://doi.org/10.1007/s00339-021-05055-x
37. A. Martí, L. Cuadra, A. Luque, Design constraints of the quantum-dot intermediate band solar cell. Phys. E Low-Dimens Syst. Nanostruct. **14**, 150–157 (2002). https://doi.org/10.1016/S1386-9477(02)00368-5
38. H. Abboudi, H. El Ghazi, A. Jorio, I. Zorkani, Impurity-related photovoltaic efficiency of (In, Ga)N/GaN quantum well-single intermediate band solar cell considering heavy hole impact. Superlattices Microstruct. **150**, 106756 (2021). https://doi.org/10.1016/j.spmi.2020.106756